

Journal of Materials Chemistry A

Accepted Manuscript



This is an *Accepted Manuscript*, which has been through the Royal Society of Chemistry peer review process and has been accepted for publication.

Accepted Manuscripts are published online shortly after acceptance, before technical editing, formatting and proof reading. Using this free service, authors can make their results available to the community, in citable form, before we publish the edited article. We will replace this *Accepted Manuscript* with the edited and formatted *Advance Article* as soon as it is available.

You can find more information about *Accepted Manuscripts* in the [Information for Authors](#).

Please note that technical editing may introduce minor changes to the text and/or graphics, which may alter content. The journal's standard [Terms & Conditions](#) and the [Ethical guidelines](#) still apply. In no event shall the Royal Society of Chemistry be held responsible for any errors or omissions in this *Accepted Manuscript* or any consequences arising from the use of any information it contains.

Tunable design of layered CuCo_2O_4 nanosheets@ MnO_2 nanoflakes core/shell arrays on Ni foam for high-performance supercapacitors

Min Kuang^a, Xiao Ying Liu^a, Fan Dong^b, Yu Xin Zhang^{a,c,*}

^a College of Materials Science and Engineering, Chongqing University, Chongqing 400044, P.R. China

^b Chongqing Key Laboratory of Catalysis and Functional Organic Molecules, College of Environmental and Biological Engineering, Chongqing Technology and Business University, Chongqing 400067, P. R. China

^c National Key Laboratory of Fundamental Science of Micro/Nano-Devices and System Technology, Chongqing University, Chongqing 400044, P.R. China

*E-mail: zhangyuxin@cqu.edu.cn

Fax: +8623 6510 4131; Tel: +8623 6510 4131

Abstract

A facile and scalable method is developed to synthesize layered CuCo_2O_4 nanosheets@ MnO_2 nanoflakes core/shell arrays (CuCo_2O_4 @ MnO_2 NSCs) on Ni foam. Interestingly, the superstructures of core include well-arranged micrometer length rectangular two-dimensional (2D) nanosheets with high pore volume. Subsequently, MnO_2 nanoflakes are vertically grown on CuCo_2O_4 nanosheets to form core/shell architecture. The electrochemical measurements demonstrate a high specific capacitance of 416 F g^{-1} at the current density of 1 A g^{-1} with excellent rate capability and remarkable cycling stability (92.1% retention after 4200 cycles). Impressively, the optimized CuCo_2O_4 @ MnO_2 //AG ACS cell can be cycled reversibly in a wide voltage region as high as 2.0 V and exhibits a specific capacitance of 78 F g^{-1} at a current density of 1 A g^{-1} with a maximum energy density of 43.3 Wh kg^{-1} . These encouraging results suggest that such unique CuCo_2O_4 @ MnO_2 NSCs architecture could be considered as one of the most promising candidates for energy storage devices with higher energy density delivery.

Keywords: supercapacitors; core/shell; manganese dioxide; electrochemical performance

Introduction

The growing concerns about capable mobile devices combined with the more generally hybrid-electric cars call for not only new electrode materials, but also more cost-effective energy storage devices with higher energy density and power density delivery.¹⁻³ Supercapacitors have attracted intensive attention owing to their remarkable characteristics (such as extremely power density, excellent reversibility, fast rates of charge/discharge, long cycle life and wide range of working temperature), although they are now restricted by its connatural low energy density characteristic.⁴ Thus, many efforts have been devoted to enhance the energy density of supercapacitors without deteriorating the long cycling life and high power density characteristics. It is quite evident that the energy density can be improved by optimizing the specific capacitance and voltage window of electrode.⁵ More recently, the effective methods to improve both the specific capacitance and voltage window are to fabricate composite dioxide with complex configuration, which provide effective utilization of active materials, and assemble asymmetric supercapacitors (ACSSs), which increase the device maximum operating voltage by combining the advantages of the two electrodes.⁶⁻⁹ Both of them are essentially determined by the electrode, thus fabricating the electrode materials is most crucial for supercapacitors to achieve the devices of high energy and power density.

Among various electrode materials explored for supercapacitors, manganese dioxide (MnO_2) is considered as a promising electrode material owing to their ideal capacitive performance, wide potential window in aqueous electrolyte, natural abundance and low cost.¹⁰⁻¹² However, the MnO_2 -based electrode materials reported previously exhibit much lower specific capacitance than expected as a result of the low electrical conductivity and volume shrinkage during fast charge/discharge process.¹³⁻¹⁶ An emerging efficient strategy to enhance the capacitive performance of

the electrode is to design smart integrated configurations allied with various materials on conductive substrates as binder- and conducting agent-free electrodes.¹⁷ Compared with single-component materials, composite oxides with complex architectures can not only provide fast pathways and abundant electroactive surface sites to harvest a maximum electrochemical performance, but also make full use of the synergistic effect of different component to optimize the electrode's properties.¹⁸ For example, Jiang et al.³ described the design of Ni(OH)₂@MnO₂ core-shell nanostructures with high specific capacitance and rate capability ; Yu et al.¹¹ demonstrated the fabrication of NiCo₂O₄@MnO₂ core/shell arrays with an improved capacitance; Wang et al.¹⁹ presented the construction of hybrid CuCo₂O₄@MnO₂ nanowires on carbon cloth with long cycling life. Although these results have manifested the feasibility of this strategy, the achieved electrochemical performances, including specific capacitance, rate capability, energy density and cycling stability, have been largely unsatisfactory. Therefore, it is necessary to fabricate novel materials or complex architecture with ideal capacitive performance.

In addition, as a typical transition-metal oxide, Co₃O₄ has also been widely investigated as possible candidates to supercapacitors, and verified promising capacitive behavior.^{18, 20, 21} Nonetheless, partial replacement of Co with eco-friendly and cost-effective element to develop a spinel structure compound could be demonstrate to be better owing to the toxic characteristic and high-cost of cobalt.²²⁻²⁴ CuCo₂O₄, as a ternary metallic oxide, have been studied as an anode material in supercapacitors, Li-air batteries and Li-ion batteries displaying excellent storage capabilities, demonstrating that they also possess promising capacitive behavior provided by the redox reaction and cation intercalation/deintercalation.²⁵⁻²⁷ More importantly, CuCo₂O₄ usually exhibits higher kinetics than single-component copper oxides (CuO) or cobalt oxides (Co₃O₄) during the fast redox reaction

due to their good electronic conductivity and excellent electrochemical activity.²⁸ There have been several reports on the fabrication and electrochemical investigation of hierarchical CuCo₂O₄ micro-/nanomaterials with various morphologies. For example, Pendashteh et al.²⁸ have reported cauliflower-like CuCo₂O₄ microstructures as a novel electrode material for supercapacitors which exhibited good specific capacitance (338 F g⁻¹) and high power density (22.11 KW kg⁻¹). Wang et al.²⁹ have tried to synthesize CuCo₂O₄ nanowire arrays on Ni foam for achieving relatively low specific capacitance (57.8 F g⁻¹ at 1.25 A g⁻¹). They subsequently enhanced electrochemical performance by constructing hybrid CuCo₂O₄@MnO₂ nanowires on carbon cloth to obtain a high specific capacitance (338 F g⁻¹), good rate capability and excellent cycling stability. Gu et al.³⁰ have obtained CuCo₂O₄ nanowires on a Ni wire with a higher specific capacitance and outstanding cycling stability. Thus, these attractive characteristics can make the CuCo₂O₄ micro-/nanomaterials as a promising candidate for supercapacitors with high energy and power density.

Herein, we present a facile and scalable strategy to fabricate layered CuCo₂O₄ nanosheets@MnO₂ nanoflakes core/shell arrays on Ni foam as a promising electrode for supercapacitors. The electrochemical measurements demonstrate a high specific capacitance of 416 F g⁻¹ at the current density of 1 A g⁻¹ with excellent rate capability and remarkable cycling stability (92.1% retention after 4200 cycles). Impressively, the optimized CuCo₂O₄@MnO₂//AG ACS cell can be cycled reversibly in a wide voltage region as high as 2.0 V in NaSO₄ aqueous electrolyte and exhibits a specific capacitance of 78 F g⁻¹ at a current density of 1 A g⁻¹ with a maximum energy density of 43.3 Wh kg⁻¹.

Experimental Section

All the chemicals and solvents in this study were analytical grade and used without further purification.

Preparation of layered CuCo_2O_4 nanosheets on Ni Foam (NSs)

CuCo_2O_4 nanosheets were obtained through combining a hydrothermal reaction and a thermal annealing process. In a typical synthesis, nickel foam ($\sim 5 \times 1.5$ cm) was carefully cleaned with concentrated HCl solution (~ 37 wt%) in an ultrasound bath for 2 min in order to remove NiO layer on the surface and then washed with deionized water and absolute ethanol for several times. Cobalt nitrate (2.0 mmol), copper nitrate (1.0 mmol) and urea (5 mmol) were dissolved in 35 mL deionized water and sonicated for 10 min. The as-obtained solution and nickel foam were transferred to a 50 mL Teflon-lined autoclave, which was sealed and then maintained at 120 °C for 6 h in an electric oven. Finally, the sample was annealed at 300 °C for 3 h, and the as-synthesized CuCo_2O_4 nanosheets hybrid structure was obtained.

Preparation of $\text{CuCo}_2\text{O}_4@ \text{MnO}_2$ core/shell arrays (CAs)

In a typical synthesis, a piece of nickel foam with grown CuCo_2O_4 nanosheets was put into a 50 mL Teflon-lined autoclave including 35 mL KMnO_4 solution (0.05 M). Finally, the reaction mixture was maintained at 140 °C for 24 h. After the reaction, the solution was cooled down to room temperature naturally. Then the as-obtained sample was rinsed with deionized water and absolute ethanol with the assistance of ultrasonication for 10 min, and dried at 60 °C for 4 h.

Materials characterization

The morphologies, microstructures, and compositions of the products were characterized by focused ion beam scanning electron microscopy (ZEISS AURIGA FIB/SEM) equipped with an energy dispersive X-ray spectrometer (EDX), X-ray diffraction (XRD, D/max 1200, Cu $K\alpha$) and high-resolution transmission electron microscopy (HRTEM, ZEISS LIBRA 200).

Electrochemical measurements

The electrochemical measurements of the prepared samples were carried out in a three-electrode in 1.0 M Na₂SO₄ electrolyte. Ag/AgCl electrode and platinum electrode were used as the reference electrode electrode and counter electrode, respectively. The CuCo₂O₄@MnO₂ CAs (~1×1 cm², CuCo₂O₄ mass ≈ 0.7 mg, MnO₂ mass ≈ 0.9 mg) or CuCo₂O₄ NSs (~1×1 cm², CuCo₂O₄ mass ≈ 0.7 mg) was directly used as working electrode without any binder and conductive actives. The electrochemical properties were investigated by cyclic voltammetry (CV) technique with varying the scan rate of 5-80 mV s⁻¹ at potential between -0.2 and 0.8 V. Galvanostatic charge-discharge (GCD) experiments were conducted with current densities ranged from 1 to 10 A g⁻¹ at a potential of -0.2 to 0.8 V.

Asymmetric cells

The CuCo₂O₄@MnO₂ CAs and activated graphenes (AG) were tailored with the same size and then assembled together with separator and the electrochemical measurements were performed with two-electrode stainless-steel simulation cells in 1 M NaSO₄ electrolyte. All the operating current densities were calculated based on the total weight of CuCo₂O₄@MnO₂ CAs and AG. The capacitances (C_m) of the electrodes are calculated from the GCD curves at different current densities using the Equation (1):

$$C_m = I \cdot \Delta t / m \cdot \Delta V \quad (1)$$

Where I (A) is the discharge current, m (g) is the load mass of the active materials (g), Δt (s) is the discharging time and ΔV (V) represents the discharging potential range. The electrochemical performance of the asymmetric cell was based on the capacitance obtained from the GCD curves. The energy density and power density of the asymmetric cell were calculated from Equations (2) and (3):

$$E = 0.5 \cdot C_m \cdot (\Delta V)^2 / 3.6 \quad (2)$$

$$P = E \cdot 3600 / \Delta t \quad (3)$$

where E is the energy density (Wh Kg⁻¹), P is power density (W Kg⁻¹) and Δt (s) is the total discharge time.

Results and Discussion

Our synthesizing strategy for fabricating CuCo₂O₄@MnO₂ CAs as supercapacitor electrode includes two main steps, as displayed in Fig. 1. CuCo₂O₄ NSs on nickel foam were first obtained through combining a facial hydrothermal reaction and a thermal annealing process. It is noteworthy that the three-dimensional nickel foam was acted as the current collector owing to its uniform and macropores structure, excellent electrical conductivity and large supporting area. Subsequently, the surface CuCo₂O₄ NSs was uniformly covered with a thin layer of MnO₂ nanoflakes through the heterogeneous nucleation process, and finally forming the hybrid CuCo₂O₄@MnO₂ core/shell nanostructure.

As shown in Fig. 2a, high-density layered nanosheets were uniformly fabricated on nickel foam. More interestingly, the precursor displays the layered morphology with well-arranged two-dimensional nanosheets. After the thermal annealing, the morphology of the CuCo₂O₄ NSs did not change a lot, keeping the highly layered morphology consisting of well-arranged rectangular two-dimensional nanosheets (Fig. 2b). The high-magnification SEM image (Fig. 2c) shows that the CuCo₂O₄ NSs has widths of approximately 600 nm with almost uniform micrometer length interlayer spacing. It is noteworthy that the thermal annealing process includes removal of H₂O and CO₂ from the precursor crystals so as to form the porous CuCo₂O₄ NSs, further demonstrated by the TEM image. The composition of the CuCo₂O₄ NSs has been studied by XRD (Fig. 2d). The peaks at 44°, 52° and 76°

come from the Ni foam substrate, while the remaining peaks at $2\theta = 19^\circ, 31^\circ, 37^\circ, 59^\circ$ and 65° can be well indexed to (111), (220), (311), (511) and (440) reflections of pure cubic spinel structure of CuCo_2O_4 (JPCDS No. 1-1155). Fig. 2e displays the TEM image of a single CuCo_2O_4 NSs scratched from Ni foam, giving the further information of the layered and highly porous features, coincide with the SEM observation. Moreover, this unique structure can be expected to provide a large deal of exposed surface and efficient utilization of active materials, which are crucial for electrochemical activity. The HRTEM images displayed in Fig. 2f reveal the lattice fringes with a spacing of 0.20, 0.25 and 0.29 nm correspond to (400), (311) and (220) planes, respectively, of cubic spinel CuCo_2O_4 NSs. The corresponding SAED pattern (See Supplementary information, SI-1) shows the well-defined rings which are readily ascribed to the (111), (220), (311), (400), (511) and (440) planes of cubic spinel CuCo_2O_4 NSs, respectively, verifying the CuCo_2O_4 NSs are polycrystalline with d -spacing, coincide with XRD observation (Fig. 2d).

After a 24-hour hydrothermal reaction in aqueous KMnO_4 solution, MnO_2 can be expected to grow on the surface of CuCo_2O_4 NSs through the self-decomposition of KMnO_4 solution. In Fig. 3a, the broad XRD peaks at $12^\circ, 25^\circ$ and 37° can be readily ascribed to birnessite-type $\delta\text{-MnO}_2$ (JPCDS No. 86-0666), demonstrating the formation of $\delta\text{-MnO}_2$ nanocrystalline structure. The peaks at $19^\circ, 37^\circ, 59^\circ$ and 65° are assigned to CuCo_2O_4 NSs, with $44^\circ, 52^\circ$ and 76° belonging to Ni foam. These observations indicate the presence of $\delta\text{-MnO}_2$ and CuCo_2O_4 on the Ni foam. Furthermore, the existence of manganese dioxide and copper cobaltite is also demonstrated by EDX (SI-2). As manifested in SI-2, the uniform structure is still maintained after the coating of $\delta\text{-MnO}_2$ nanoflakes on the surface of CuCo_2O_4 NSs. All of these results verify that $\text{CuCo}_2\text{O}_4@ \text{MnO}_2$ CAs have been obtained successfully through effective and simple hydrothermal reaction. The SEM images in Fig. 3b and c display the

morphology of $\text{CuCo}_2\text{O}_4@\text{MnO}_2$ CAs with different magnifications. After the hydrothermal reaction, a thick layer of $\delta\text{-MnO}_2$ nanoflakes is grown on the surface of CuCo_2O_4 NSs to form core/shell architecture. These as-obtained $\delta\text{-MnO}_2$ nanoflakes are only 20 ~ 30 nm in thickness and ~ 200 nm in lateral size. It is interesting to note that the exterior surface of CuCo_2O_4 NSs are vertically covered with ultrathin $\delta\text{-MnO}_2$ nanoflakes, which are interconnected with each other and create highly porous nanostructure with a large amount of electroactive surface sites and open spaces. The low-magnification TEM image of $\delta\text{-MnO}_2$ nanoflakes (Fig. 3d) indicates that the nanoflakes are sustaining with a smooth surface with transparent characteristic, revealing the ultrathin feature. The SAED pattern (Fig. 3d, inset) of the nanoflakes manifested the polycrystalline feature of the $\delta\text{-MnO}_2$. The HRTEM images (Fig. 3e) clearly reveals that lattice fringe spaces of 0.19 and 0.23 nm are corresponding to the (-111) and (201) plane of birnessite-type $\delta\text{-MnO}_2$, respectively. Furthermore, abundant mesopores in these ultrathin nanoflakes can be clearly observed (Fig. 3d), which can facilitate the diffusion of the electrolytes ions within the electrodes so as to further improve the electrochemical performance.

The growth process of $\delta\text{-MnO}_2$ shell is investigated by observing the morphologies at different growing stages. The SEM images of the samples at different hydrothermal reaction time are displayed in Fig. 4. Before reaction, the CuCo_2O_4 NSs are coalescent through the hydrothermal ripening, intrinsic crystal contraction, Ostwald ripening and thermal deposition process, as shown in Fig. 4a. After being dipped into the permanganate solution for 2 h (Fig. 4b), there are no nanoparticles or tiny “buds” on the smooth surface of the CuCo_2O_4 NSs. However, it is noteworthy that the interlayer spacing of the CuCo_2O_4 NSs is broadened, intercrossing three-dimensional network with more open space. When the reaction time is prolonged (6 h, Fig. 4c), the tiny “duds” begin to grow on the surface of the core

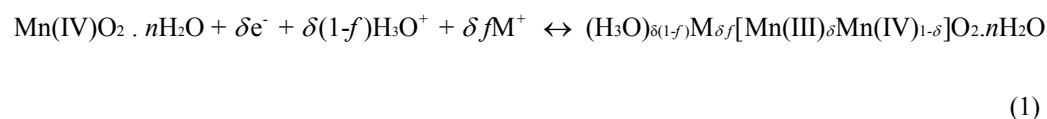
nanosheets. As the hydrothermal reaction proceeds, the δ -MnO₂ shell starts to grow up and the mass of the shell increases accordingly, resulting to less open space between each CuCo₂O₄@MnO₂ CAs. Obviously, the thickness and lateral size of the δ -MnO₂ shell can be readily modulated by tuning the hydrothermal reaction time. It is also evident that we are able to tune the architecture of the CuCo₂O₄@MnO₂ CAs.

The CV and GCD techniques were performed in three-electrode device to evaluate the electrochemical performance of the layered CuCo₂O₄@MnO₂ CAs for supercapacitors. Fig. 5a exhibits the typical CV curves of the CuCo₂O₄@MnO₂ CAs electrode (binder- and conductive agent-free electrodes) in a 1 M NaSO₄ electrolyte solution. Clearly, the CV curves at various scan rates exhibit a similar shape, indicating the ideal intralayer charge transfer and good reversibility feature.³¹ Even at a scan rate of 80 mV s⁻¹, the CV curve still displays a quasi-rectangular shape, demonstrating that this hierarchical architecture is conducive to fast redox reaction.³² The Ni foam support will assure the superior electrical conductivity of the hybrid architecture and layered CuCo₂O₄ NSs can further provide fast pathways and abundant electroactive surface sites to harvest a maximum of δ -MnO₂ shell capacitance even at a fast redox reaction. Fig. 5b shows the representative triangular-shape GCD curves of the CuCo₂O₄@MnO₂ CAs electrode. As we can see, these GCD curves display reasonably linear slopes and excellent symmetry, further indicating the ideal capacitive properties of the hierarchical CuCo₂O₄@MnO₂ CAs electrode.³³ Fig. 5c exhibits the results of GCD technique on the CuCo₂O₄ NSs and CuCo₂O₄@MnO₂ CAs electrode, which were conducted at a current density of 1 A g⁻¹. Notably, the charge/discharge time for hierarchical CuCo₂O₄@MnO₂ CAs electrode was virtually longer than the CuCo₂O₄ NSs electrode. Evidently, the hierarchical CuCo₂O₄@MnO₂ CAs electrode possess higher specific capacitance (416 F g⁻¹ and 62 F g⁻¹ for the CuCo₂O₄@MnO₂ CAs and CuCo₂O₄ NSs,

respectively), which are consistent with the CV results (SI-3). Moreover, the comparison of the specific capacitance between this work and previous reports is summarized (Table S1). The specific capacitance of CuCo₂O₄@MnO₂ CAs (based on the mass of CuCo₂O₄ and MnO₂) is much higher than many MnO₂- or CuCo₂O₄-based electrodes.²⁸⁻³⁰

Fig. 5d depicts the relationship between current density and specific capacitance. About 82.9 % of specific capacitance has been maintained when the current density increased from 1 A g⁻¹ to 8 A g⁻¹. The result further demonstrates the advantage of these hierarchical CuCo₂O₄@MnO₂ CAs.

It has been generally accepted that the capacitance of MnO₂ comes from two aspects: the fast redox reaction between the Mn(III) and Mn(IV) and the cation absorption/desorption at the material's surface.^{34,35} In other words, the III oxidation state in the MnO₂ will be oxidized to IV oxidation state of Mn during charging and then reduced to III oxidation state of Mn during discharging, accompanying the adsorption of cations at the surface of MnO₂. The process of charge/discharge can be depicted as Equation (Equ.) (1):³⁶



where M⁺ is alkali cation (such as K⁺, Na⁺ and Li⁺). Although the CuCo₂O₄ core provides good electrical conductivity and efficient utilization of active materials to enhance the electrochemical activity of the hierarchical core/shell system, the charge storage mechanism of CuCo₂O₄ materials is different from MnO₂ materials, which finally exacerbates the electrochemical properties in neutral electrolyte. The electrochemical reaction of CuCo₂O₄ materials is usually written as follows:^{25, 30, 37}





This indicates that the alkaline electrolyte is more beneficial to redox reaction of CuCo_2O_4 materials. For comparison, the CV and GCD techniques were also performed in 2 M KOH electrolyte solution (SI-4). All of the CV curves display a pair of redox peaks, which demonstrates the pseudocapacitive behavior of the CuCo_2O_4 caused by Faradaic reactions of the reversible $\text{Co}^{4+}/\text{Co}^{3+}$ and $\text{Cu}^{2+}/\text{Cu}^+$ couple.³⁰ Note that the GCD curves are nearly symmetrical, revealing superior electrochemical capacitive features and high charge/discharge coulombic efficiency in the hybrid electrode.³⁸ Remarkably, the nonlinear characteristic of these GCD curves further manifests the pseudocapacitive properties of this hybrid $\text{CuCo}_2\text{O}_4@\text{MnO}_2$ CAs electrode. Moreover, the hybrid $\text{CuCo}_2\text{O}_4@\text{MnO}_2$ CAs electrode also exhibited a high specific capacitance of 405 F g^{-1} even at basic electrolyte. It is evident that our as-obtained hybrid $\text{CuCo}_2\text{O}_4@\text{MnO}_2$ CAs electrode is not only appropriate for neutral electrolyte, but are also applied in basic electrolyte, both indicating an amusing electrochemical performance.

The cycling stability of the hybrid $\text{CuCo}_2\text{O}_4@\text{MnO}_2$ CAs electrode in a 1 M Na_2SO_4 electrolyte is another important aspect for practical viability of the supercapacitor. Fig. 6 shows the specific capacitance as function of cycle number plots at a high current density of 8 A g^{-1} for more than 4200 cycles. Interestingly, clear improvement in the specific capacitance of the hybrid electrode is observed during the initial 210 cycles, which can be mainly ascribed to the activation of electrode, and subsequently decreases slightly.³⁹ Importantly, the hybrid electrode possesses an excellent cycling stability with only 7.4% loss after 4200 cycles. This superior electrochemical stability can be mainly explained by the layered structure of the core, which can not only provide quicker infiltration process of electrolyte by decreasing the transmission time of ions penetrating into the

layered matrix, but also accommodates the possible strain arising caused by high rate absorption/desorption of ions. Moreover, the synergic effect between CuCo_2O_4 and MnO_2 can further alleviate the structure damage of the MnO_2 shell layer due to the volume change and redox reaction during charge/discharge process, and thus enhance the structural stability and electrochemical reversibility of the hybrid $\text{CuCo}_2\text{O}_4@\text{MnO}_2$ CAs electrode, as illustrated in the inset of the Fig. 6.

To further evaluate the practical viability of such hybrid $\text{CuCo}_2\text{O}_4@\text{MnO}_2$ CAs, an asymmetric supercapacitor (ASC) cell was constructed by using $\text{CuCo}_2\text{O}_4@\text{MnO}_2$ CAs as the positive electrode and AG on the Ni foam as the negative electrode with the separator and 1 M Na_2SO_4 electrolyte (denoted as $\text{CuCo}_2\text{O}_4@\text{MnO}_2//\text{AG}$). Furthermore, to obtain the optimized electrochemical performance of $\text{CuCo}_2\text{O}_4@\text{MnO}_2//\text{AG}$ ACS cell, it is necessary to optimize the mass ratio of positive and negative electrode ($m(\text{CuCo}_2\text{O}_4@\text{MnO}_2)/m(\text{AG})$), and based on the balance of charge/discharge ($Q_+ = Q_-$) between the two electrodes, the $m(\text{CuCo}_2\text{O}_4@\text{MnO}_2)/m(\text{AG})$ can be optimized to be 0.32 (SI-5). The as-assembled $\text{CuCo}_2\text{O}_4@\text{MnO}_2//\text{AG}$ ACS cell with optimal mass ratio was investigated at different voltage windows in a 1 M Na_2SO_4 solution at 40 mV s^{-1} to estimate the optimal operating potential window of $\text{CuCo}_2\text{O}_4@\text{MnO}_2//\text{AG}$ ACS cell, and the results are exhibited in Fig. 7a. The as-assembled $\text{CuCo}_2\text{O}_4@\text{MnO}_2//\text{AG}$ ACS cell displays an ideal capacitive behavior with quasi-rectangular CV curve even when the operating window extends to 2.0 V, meaning that the ACS cell is extremely stable under such condition.⁴⁰ Therefore, the wide voltage window of 2.0 V is used as the cells potential to further study the overall electrochemical performance of the $\text{CuCo}_2\text{O}_4@\text{MnO}_2//\text{AG}$ ACS cell. Then, CV curves of ACS cell at various scan rates of 5 - 60 mV s^{-1} are exhibited in Fig. 7b. All of these CV curves display a nearly rectangular-like shape without any obvious redox peaks, demonstrating an excellent

rate capability for power devices.⁴¹ Fig. 7c exhibits the GCD profiles at different current densities. As shown in Fig. 7c, all of these charge/discharge lines are almost symmetric, further suggesting excellent capacitive behavior for the ACS cell. Moreover, the GCD curves are also used to evaluate the energy and power feature of the $\text{CuCo}_2\text{O}_4@\text{MnO}_2//\text{AG}$ ACS cell, a Ragone plot is shown in Fig. 7d. Note that a high energy density of 43.3 Wh kg^{-1} can be gained at a power density of 287 W kg^{-1} and still maintains 26 Wh kg^{-1} even at a high power density of 2989 W kg^{-1} , which is higher than previously reported systems such as $\text{MnO}_2/\text{SiO}_2//\text{MnO}_2/\text{SiO}_2$ symmetric supercapacitor, $\text{NiCo}_2\text{O}_4\text{-MnO}_2//\text{AG}$ ASC, $\text{CNF}/\text{MnO}_2//\text{AG}$ ASC and $\text{CNT}/\text{MnO}_2/\text{GR}/\text{CNT}/\text{PANI}$ ASC.^{8, 9, 42, 43} These interesting results demonstrate the ideal capacitive behavior of the $\text{CuCo}_2\text{O}_4@\text{MnO}_2//\text{AG}$ ACS cell and undoubtedly pave the way for researchers to obtain superior electrochemical performance energy storage devices based on binder- and conductive agent-free electrode.

Conclusion

In conclusion, a facile, controllable and surfactant-free hydrothermal technique has been developed to synthesize layered CuCo_2O_4 nanosheets@ MnO_2 nanoflakes core/shell arrays with unique hierarchical architecture and excellent porosity. The size of MnO_2 nanoflakes can be readily controlled by adjusting the hydrothermal reaction time. The electrochemical measurement exhibited a high specific capacitance of 416 F g^{-1} at the current density of 1 A g^{-1} with remarkable cycling stability (92.4% retention after 4200 cycles), good reversibility feature and excellent rate capability. Impressively, the optimized $\text{CuCo}_2\text{O}_4@\text{MnO}_2//\text{AG}$ ACS cell can be cycled reversibly in a wide voltage region as high as 2.0 V and exhibits a specific capacitance of 78 F g^{-1} at a current density of 1 A g^{-1} with a maximum energy density of 43.3 Wh kg^{-1} . These results suggest that the hybrid $\text{CuCo}_2\text{O}_4@\text{MnO}_2$ CAs is expected to be an effective electrode for supercapacitors with excellent

electrochemical properties.

Acknowledgement. The authors gratefully acknowledge the financial supports provided by National Natural Science Foundation of China (Grant no. 51104194), International S&T Cooperation Projects of Chongqing (CSTC2013ghz90001), National Key laboratory of Fundamental Science of Micro/Nano-device and System Technology (2013MS06, Chongqing University), State Education Ministry and Fundamental Research Funds for the Central Universities (Project no. CDJZR14135501, Chongqing University, PR China).

References

- [1] J. Liu, J. Jiang, M. Bosman, H.J. Fan, *J. Mater. Chem.*, 2012, **22**, 2419-2426.
- [2] C. Liu, Z. Yu, D. Neff, A. Zhamu, B.Z. Jang, *Nano Lett.*, 2010, **19**, 4863-4868.
- [3] H. Jiang, C. Li, T. Sun, J. Ma, *Chem. Commun.*, 2012, **48**, 2606-2608.
- [4] J. Jiang, Y. Li, J. Liu, X. Huang, C. Yuan, X.W. Lou, *Adv. Mater.*, 2012, **24**, 5166-4180.
- [5] Z. Fan, J. Yan, T. Wei, L. Zhi, G. Ning, T. Li, F. Wei, *Adv. Funct. Mater.*, 2011, **21**, 2366-2375.
- [6] J.-G. Wang, Y. Yang, Z.-H. Huang, F. Kang, *Electrochim. Acta*, 2011, **56**, 9240-9247.
- [7] Q. Li, Z.L. Wang, G.R. Li, R. Guo, L.X. Ding, Y.X. Tong, *Nano Lett.*, 2012, **12**, 3803-3807.
- [8] Y. Jin, H. Chen, M. Chen, N. Liu, Q. Li, *ACS Appl. Mater. Interfaces*, 2013, **5**, 3408-3416.
- [9] J.-G. Wang, Y. Yang, Z.-H. Huang, F. Kang, *Carbon*, 2013, **61**, 190-199.
- [10] X. Xie, C. Zhang, M.B. Wu, Y. Tao, W. Lv, Q.H. Yang, *Chem. Commun.*, 2013, **49**, 11092-11092A.
- [11] L. Yu, G. Zhang, C. Yuan, X.W. Lou, *Chem. Commun.*, 2013, **49**, 137-139.
- [12] X. Lu, M. Yu, G. Wang, T. Zhai, S. Xie, Y. Ling, Y. Tong, Y. Li, *Adv. Mater.*, 2013, **25**, 267-272.
- [13] H. Jiang, J. Ma, C. Li, *J. of Mater. Chem.*, 2012, **22**, 16939-16942.
- [14] G. Zhu, Z. He, J. Chen, J. Zhao, X. Feng, Y. Ma, Q. Fan, L. Wang, W. Huang, *Nanoscale*, 2014, **6**, 1079-1085.
- [15] M. Liu, L. Gan, W. Xiong, Z. Xu, D. Zhu, L. Chen, *J. Mater. Chem. A*, 2014, **2**, 2555-2562.
- [16] J.-X. Feng, Q. Li, X.-F. Lu, Y.-X. Tong, G.-R. Li, *J. Mater. Chem. A*, 2014, **2**, 2985-2992.
- [17] L. Jiang, R. Zou, W. Li, J. Sun, X. Hu, Y. Xue, G. He, J. Hu, *J. Mater. Chem. A*, 2013, **1**, 478-481.
- [18] G. Zhang, T. Wang, X. Yu, H. Zhang, H. Duan, B. Lu, *Nano Energy*, 2013, **2**, 586-594.
- [19] Q. Wang, J. Xu, X. Wang, B. Liu, X. Hou, G. Yu, P. Wang, D. Chen, G. Shen, *ChemElectroChem*, 2014, **2**, 559-564.
- [20] L. Zhang, X. Zhao, W. Ma, M. Wu, N. Qian, W. Lu, *CrystEngComm*, 2013, **15**, 1389-1396.
- [21] H. Xia, D. Zhu, Z. Luo, Y. Yu, X. Shi, G. Yuan, J. Xie, *Sci. Rep.*, 2013, **3**, 2978-2985.
- [22] W. Li, K. Xu, G. Song, X. Zhou, R. Zou, J. Yang, Z. Chen, J. Hu, *CrystEngComm*, 2014, **16**, 2335-2339.
- [23] D. Cai, B. Liu, D. Wang, L. Wang, Y. Liu, H. Li, Y. Wang, Q. Li, T. Wang, *J. Mater. Chem. A*, 2014, **2**, 4954-4960.
- [24] S. Wang, J. Pu, Y. Tong, Y. Cheng, Y. Gao, Z. Wang, *J. Mater. Chem. A*, 2014, **2**, 5434-5440.

- [25] A. Pendashteh, S.E. Moosavifard, M.S. Rahmanifar, Y. Wang, M.F. El-Kady, R.B. Kaner, M.F. Mousavi, *Chem. Mater.*, 2015, **27**, 3919-3926.
- [26] Y. Liu, L.-J. Cao, C.-W. Cao, M. Wang, K.-L. Leung, S.-S. Zeng, T. Hung, C. Chung, Z.-G. Lu, *Chem. Commun.*, 2014, **50**, 14635-14638.
- [27] W. Kang, Y. Tang, W. Li, Z. Li, X. Yang, J. Xu, C.-S. Lee, *Nanoscale*, 2014, **6**, 6551-6556.
- [28] A. Pendashteh, M.S. Rahmanifar, R.B. Kaner, M.F. Mousavi, *Chem. Commun.*, 2014, **50**, 1972-1975.
- [29] Q. Wang, J. Xu, X. Wang, B. Liu, X. Hou, G. Yu, P. Wang, D. Chen, G. Shen, *ChemElectroChem*, 2014, **1**, 559-564.
- [30] S. Gu, Z. Lou, X. Ma, G. Shen, *ChemElectroChem*, 2015, **2**, 1042-1047.
- [31] S. Park, I. Nam, G.P. Kim, J.W. Han, J. Yi, *ACS Appl. Mater. Interfaces*, 2013, **5**, 9908-9912.
- [32] Y. Luo, D. Kong, J. Luo, S. Chen, D. Zhang, K. Qiu, X. Qi, H. Zhang, C.M. Li, T. Yu, *RSC Adv.*, 2013, **3**, 14413-14422.
- [33] L. Peng, X. Peng, B. Liu, C. Wu, Y. Xie, G. Yu, *Nano Lett.*, 2013, **13**, 2151-2157.
- [34] X. Xie, C. Zhang, M.B. Wu, Y. Tao, W. Lv, Q.H. Yang, *Chem. Commun.*, 2013, **49**, 11092-11094.
- [35] H.-Q. Wang, Z.-S. Li, Y.-G. Huang, Q.-Y. Li, X.-Y. Wang, *J. Mater. Chem. A*, 2010, **20**, 3883-3889.
- [36] C.-H. Wang, H.-C. Hsu, J.-H. Hu, *J. Power Sources*, 2014, **249**, 1-8.
- [37] M.C. Liu, L.B. Kong, C. Lu, X.M. Li, Y.C. Luo, L. Kang, *ACS Appl. Mater. Interfaces*, 2012, **4**, 4631-4636.
- [38] X. Liu, S. Shi, Q. Xiong, L. Li, Y. Zhang, H. Tang, C. Gu, X. Wang, J. Tu, *ACS Appl. Mater. Interfaces*, 2013, **5**, 8790-8795.
- [39] H.W. Shim, A.H. Lim, J.C. Kim, E. Jang, S.D. Seo, G.H. Lee, T.D. Kim, D.W. Kim, *Sci. Rep.*, 2013, **3**, 2325-2333.
- [40] S. Wu, W. Chen, L. Yan, *J. Mater. Chem. A*, 2014, **2**, 2765-2772.
- [41] P. Yang, Y. Li, Z. Lin, Y. Ding, S. Yue, C.P. Wong, X. Cai, S. Tan, W. Mai, *J. Mater. Chem. A*, 2014, **2**, 595-599.
- [42] Y.X. Zhang, M. Huang, F. Li, X.L. Wang, Z.Q. Wen, *J. Power Sources*, 2014, **246**, 449-456.
- [43] M. Kuang, Z.Q. Wen, X.L. Guo, S.M. Zhang, Y.X. Zhang, *J. Power Sources*, 2014, **270**, 426-433.

Figure 1 Schematic diagram illustrating the synthesis procedure of hierarchical $\text{CuCo}_2\text{O}_4@\text{MnO}_2$ NSCs on Ni foam.

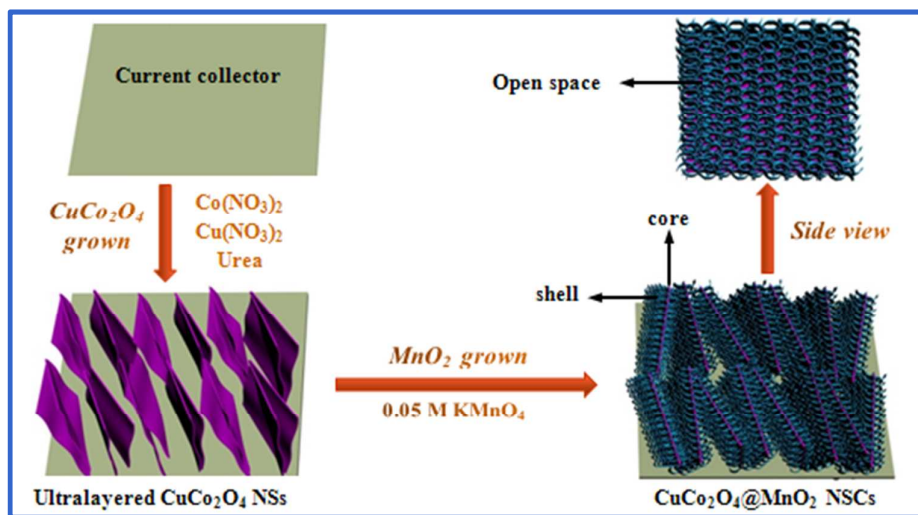


Figure 2 (a) SEM images of CuCo_2O_4 NSs before annealing (the insert shows the large-area view); (b-c) SEM images of CuCo_2O_4 NSs on Ni foam; (d) XRD pattern of CuCo_2O_4 NSs on Ni foam; (e) TEM and (f) HRTEM images of pure CuCo_2O_4 NSs.

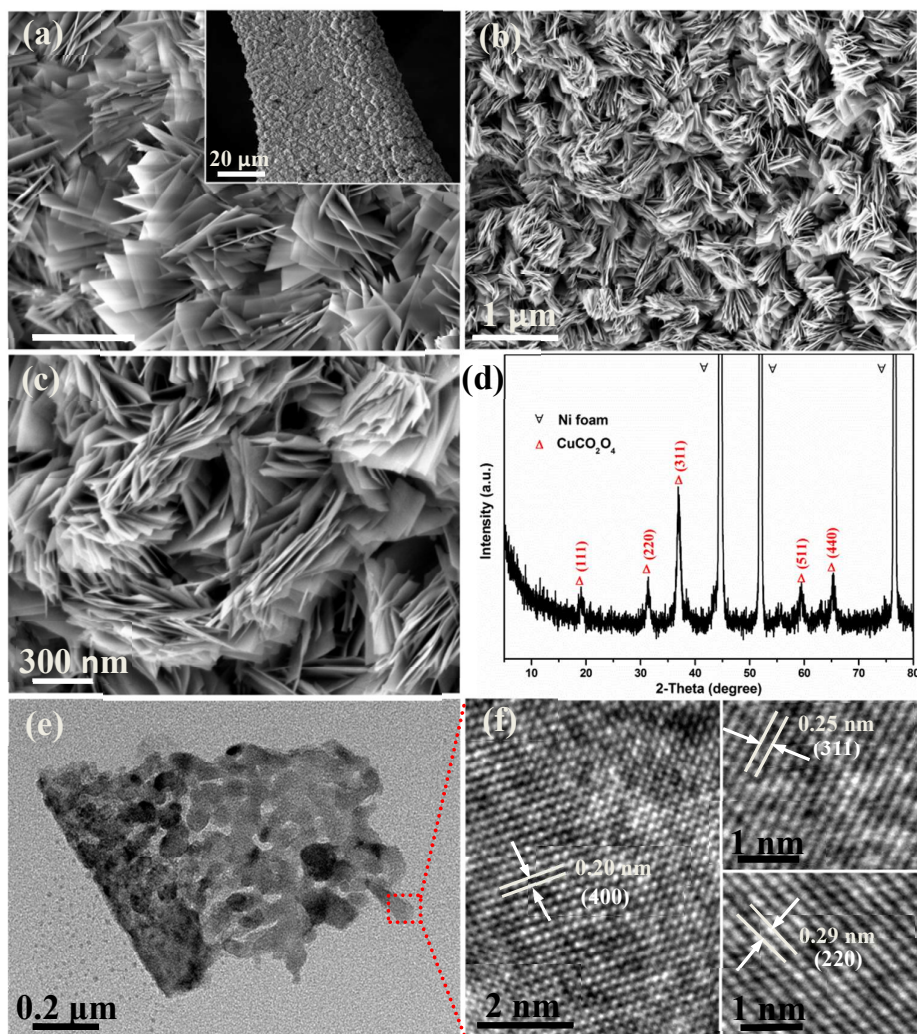


Figure 3 (a) XRD pattern of $\text{CuCo}_2\text{O}_4@\text{MnO}_2$ NSCs; (b-c) SEM images of the as-prepared $\text{CuCo}_2\text{O}_4@\text{MnO}_2$ NSCs; (d) TEM image of MnO_2 nanoflakes scratched from hierarchical heterostructure, the inset is the corresponding SAED pattern; (e) HRTEM of MnO_2 nanoflakes.

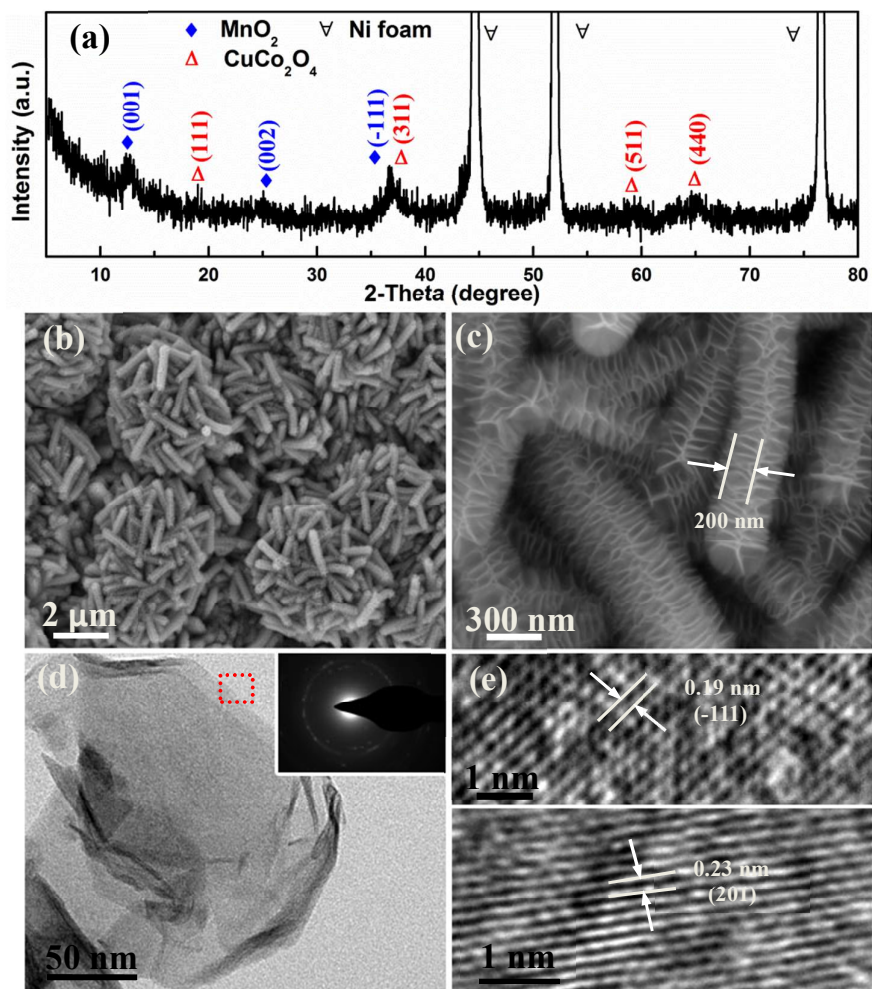


Figure 4 SEM images of $\text{CuCo}_2\text{O}_4@\text{MnO}_2$ core/shell arrays obtained at different reaction time: (a) 0 h; (b) 2 h; (c) 6 h; (d) 12 h; (e) 24 h; (f) 30 h;

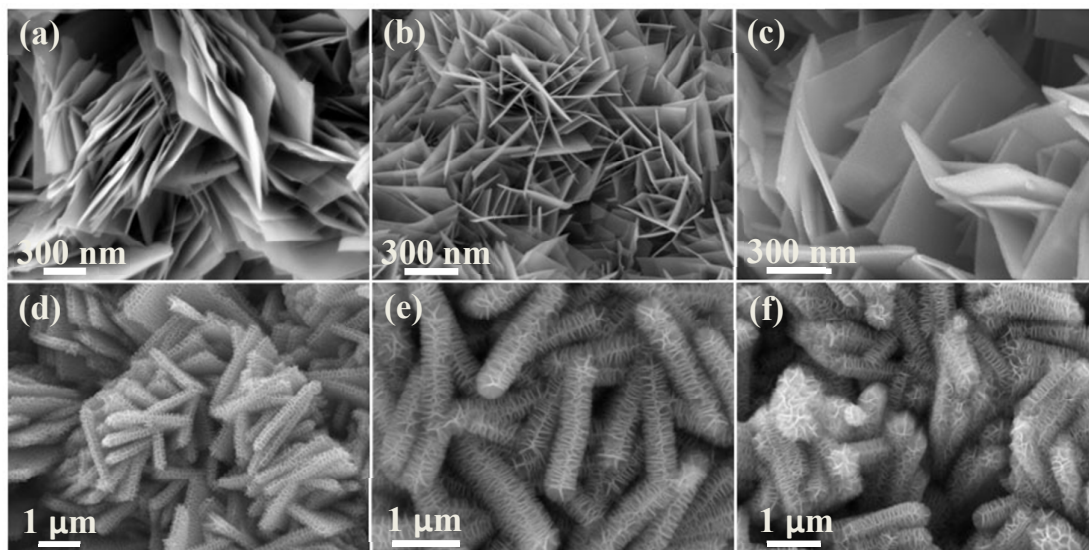


Figure 5 (a) Cyclic voltammograms of the $\text{CuCo}_2\text{O}_4@\text{MnO}_2$ NSCs at different scan rates; (b) Galvanostatic charge-discharge of the $\text{CuCo}_2\text{O}_4@\text{MnO}_2$ NSCs at various current densities; (c) Galvanostatic charge-discharge of the CuCo_2O_4 NSs and $\text{CuCo}_2\text{O}_4@\text{MnO}_2$ NSCs; (d) Current density dependence of the specific capacitance of the $\text{CuCo}_2\text{O}_4@\text{MnO}_2$ NSCs.

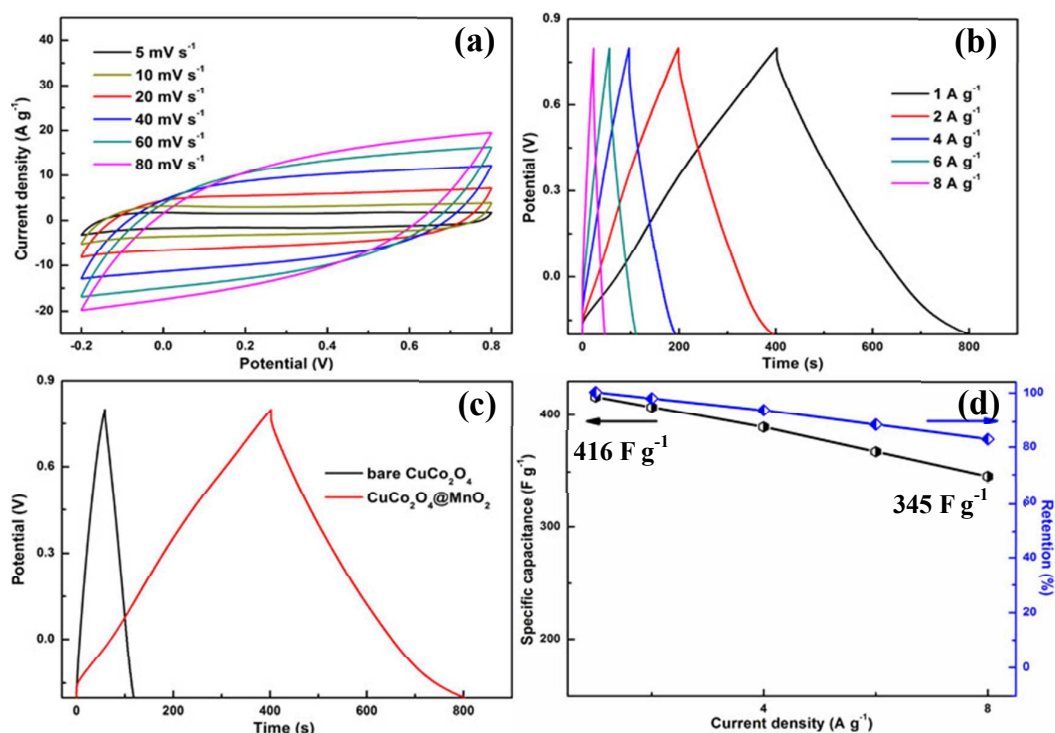


Figure 6 Cycling performance of $\text{CuCo}_2\text{O}_4@\text{MnO}_2$ NSCs at current density of 8 A g^{-1} . The inset shows the schematic of the charge storage advantage of this hierarchical architecture.

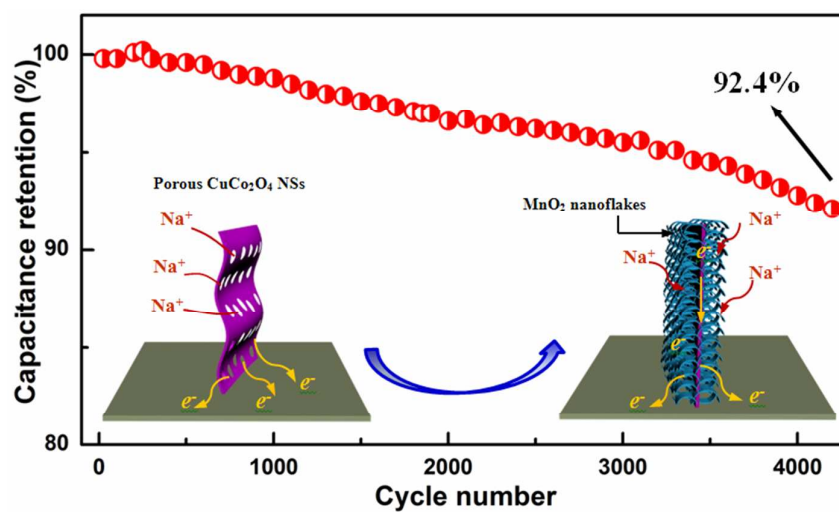


Figure 7 (a) Cyclic voltammograms of the $\text{CuCo}_2\text{O}_4@\text{MnO}_2//\text{AG}$ ASC cell measured at different potential windows; (b) Cyclic voltammograms at different scan rates; (c) Charge-discharge curves of different current densities; (d) a Ragone plot of the $\text{CuCo}_2\text{O}_4@\text{MnO}_2//\text{AG}$ ASC cell.

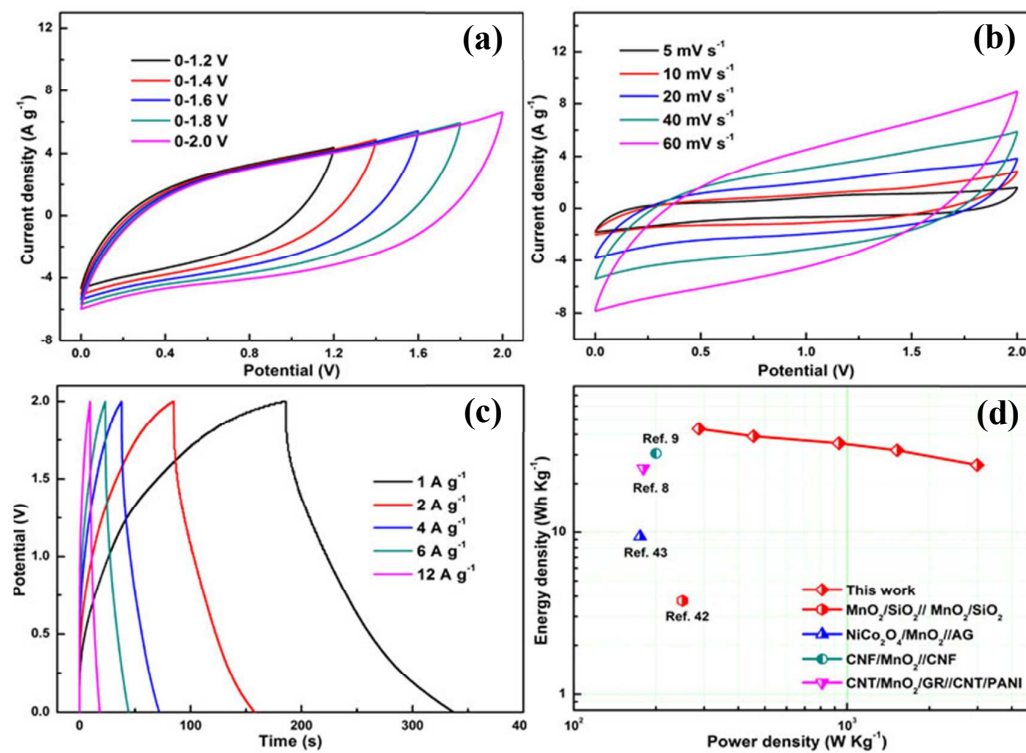
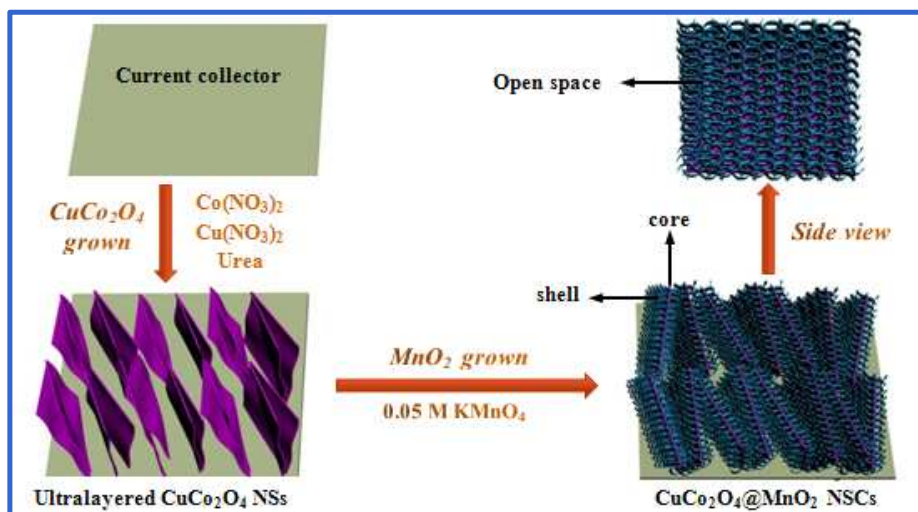


Table of content

**Tunable design of layered CuCo_2O_4 nanosheets@ MnO_2 nanoflakes core/shell arrays on Ni foam for high-performance supercapacitors**

Min Kuang, Xiao Ying Liu, Fan Dong, Yu Xin Zhang

Layered CuCo_2O_4 nanosheets@ MnO_2 nanoflakes core/shell arrays ($\text{CuCo}_2\text{O}_4@ \text{MnO}_2$ NSCs) on Ni foam have been uniformly synthesized by fine tuning the operation temperature, exhibiting superior capacitance and excellent electrochemical performance stability.